Charged Particle and Photon Interactions with Matter

Recent Advances, Applications, and Interfaces

Edited by
Yoshihiko Hatano
Yosuke Katsumura
A. Mozumder

CRC Press
Taylor & Francis Group
Boca Raton London New York

CRC Press is an imprint of the
Taylor & Francis Group, an **informa** business

CRC Press
Taylor & Francis Group
6000 Broken Sound Parkway NW, Suite 300
Boca Raton, FL 33487-2742

Printed in the United States of America on acid-free paper
10 9 8 7 6 5 4 3 2 1

International Standard Book Number: 978-1-4398-1177-1 (Hardback)

Visit the Taylor & Francis Web site at
http://www.taylorandfrancis.com

and the CRC Press Web site at
http://www.crcpress.com

5 Generalized Oscillator Strength Distribution of Liquid Water

Hisashi Hayashi
Japan Women's University
Tokyo, Japan

Yasuo Udagawa
Tohoku University
Sendai, Japan

CONTENTS

5.1 Introduction 87
5.2 Photoabsorption and Optical Oscillator Strength 88
5.3 Inelastic X-Ray Scattering and Generalized Oscillator Strength 91
5.4 Inelastic Electron Scattering and Generalized Oscillator Strength 93
5.5 GOS Measurements by IXS 94
5.6 Optical Limit 96
5.7 Comparison of GOS from EELS and IXS 99
5.8 Bethe Surface of Liquid Water 100
5.9 Concluding Remarks 101
Acknowledgments 102
References 102

5.1 INTRODUCTION

Water is the most common liquid substance on the earth's surface. Many fundamental processes, in particular those related to the development of life, take place in aqueous solutions. Accordingly, water is the most extensively studied liquid from theoretical as well as experimental points of view; several chapters of this book have the word "liquid water" in their title. Nevertheless, our knowledge about liquid water is far from complete; even now there is a debate on such a fundamental issue as to whether a water molecule is hydrogen-bonded with two other molecules or four in the liquid state (Smith et al., 2004; Wernet et al., 2004).

The optical properties of liquid water in the vacuum ultraviolet (VUV) region, like extinction coefficient (κ), refractive index (n), and reflectivity (R), are some of those which are not fully explored in spite of their importance. They all depend on photon energy, $\hbar\omega$, and are connected with each other and also to the complex dielectric response function ($\varepsilon(\omega) = \varepsilon_1(\omega) + i\varepsilon_2(\omega)$) by the following equations: $\varepsilon(\omega)^{1/2} = n + i\kappa$ and $R = [(n-1)^2 + \kappa^2]/[(n+1)^2 + \kappa^2]$. It is the dielectric response function that governs interactions between matter and photons or charged particles, which is the theme of this chapter. If one of those optical or dielectric properties is known for a wide energy range, not only can other optical properties be calculated, but also various other physical properties can be evaluated

(Inokuti, 1983; Williams et al., 1991). For example, the mean excitation energy of a material, the most important quantity required to describe the interaction with ionizing radiations, can be calculated on absolute scale. Unfortunately, such studies have been hampered by the lack of optical data in the VUV. To the best of our knowledge, optical data available in this energy region are a series of reflectance measurements at Oak Ridge (Painter et al., 1969; Kerr et al., 1971, 1972; Heller et al., 1974), but they are not wide enough, only up to 26 eV, and it has been estimated that the measurements are accurate to perhaps 30% (Kutcher and Green, 1976).

The dielectric response function ε is in fact a function of momentum transfer q also, and should be expressed as $\varepsilon(q,\omega)$. Not only are the available optical data not wide enough, but also what reflectance measurements provide are merely $\varepsilon(0,\omega)$, because the momentum of a VUV photon is very small. If $\varepsilon(q,\omega)$ of a medium is known over a wide energy and momentum range, the interaction of a charged particle with the medium can be fully understood. Such quantities as the mean free path of charged particles, cross sections for various interactions, and energy deposition, all of which are crucial in radiation chemistry/biology in vivo but are difficult to determine experimentally, can be evaluated. They ultimately lead to a track-structure analysis, which is one of the main subjects of radiation research as well as that of the previous version of this book (Nikjoo and Uehara, 2003; Nikjoo et al., 2006). Hence, many efforts have been made to estimate ω and q-dependence of $\varepsilon(q,\omega)$ of liquid water. In most of such studies, the Tennessee group's $\varepsilon(0,\omega)$ are extrapolated to a higher energy region and combined with some assumptions to extend them to finite momentum transfers (Dingfelder et al., 1998). Lacking experimental results to compare with, it has not been possible to evaluate how accurate those calculations are.

Experimentally, q-dependence of dielectric functions $\varepsilon(q,\omega)$ can be determined on gases and solids with inelastic electron scattering or electron energy loss spectroscopy (EELS) (Bonham and Fink, 1974; Egerton, 1996). For example, Lassettre et al. and Takahashi et al. have made extensive studies about dielectric functions of gaseous water (Lassettre and Skerbele, 1974; Lassettre and White, 1974; Takahashi et al., 2000) and Daniels of solid water and ice (Daniels, 1971). However, because of experimental difficulties, EELS measurements have never been carried out on volatile liquids like water.

We have pointed out that inelastic x-ray scattering (IXS) is free from difficulties inherent to optical as well as EELS measurements, the most serious of which is the need of vacuum, and can provide $\varepsilon(q,\omega)$ of volatile liquids for a wide energy and momentum-transfer range (Watanabe et al., 1997, 2000; Hayashi et al., 1998; Hayashi et al., 2000). IXS studies do not require target materials to be placed in vacuum and hence volatile liquids can be studied. Since momentum of a hard x-ray photon is large, q-dependence can easily be determined by changing the scattering angle. In the following, the manner in which photoabsorption is related to the interaction between charged particles and materials is described first, then the principles of IXS and EELS are reviewed, and finally IXS studies on liquid water are detailed.

5.2 PHOTOABSORPTION AND OPTICAL OSCILLATOR STRENGTH

It is well known that there is a close connection between the interaction of fast moving charged particles with a material and photoabsorption (Ritchie, 1982; Inokuti, 1986). In order to understand the relation heuristically, let us consider the following model depicted in Figure 5.1, where a particle with charge ze and velocity v is traveling along near an atom or a molecule with an impact parameter b. The particle exerts an electric field upon the target. Although the electric field has two components, as illustrated in the figure, only $E_\perp$ is important because $E_\parallel$ changes its sign at the distance of closest approach ($t = 0$), and as a result, the effect of $E_\parallel$ almost vanishes if integrated over the whole period. The electric field $E_\perp$ has a bell-shaped distribution in time and a simple calculation shows that its FWHM is about $2.6b/v$. Suppose the particle is an electron with a kinetic energy of 10 keV and $b = 1$ nm; the velocity v is calculated to be 6×10^7 m/s and hence the FWHM of the bell is 4×10^{-17} s, short enough to approximate the electric field as a δ-function in time. From the Fourier principle, a δ-function-like electric field in the time domain is equivalent to white light in the frequency domain. That is, the effect of the fast charged particle traveling nearby is almost the same as that of white light illuminated on the target.

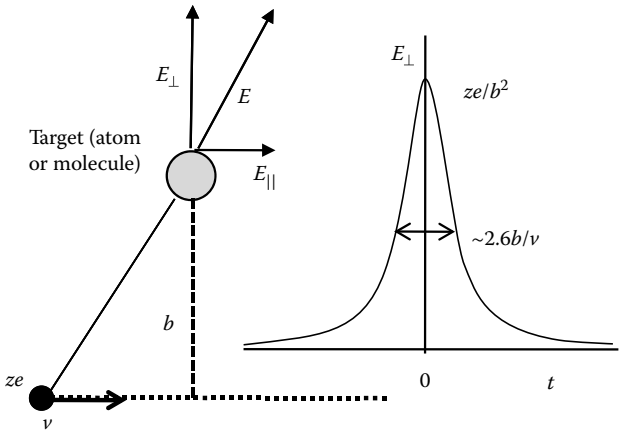

FIGURE 5.1 A particle with charge ze and velocity v passes by a target at an impact parameter b, and exerts the electric field E that depends on time t. The two components of E are given by $E_\perp = zeb/(v^2t^2 + b^2)^{3/2}$ and $E_{||} = zevt/(v^2t^2 + b^2)^{3/2}$.

The interaction between white light and a target results in an absorption of a part of the white light, accompanied by excitation of the target. From the time-dependent perturbation theory, the absorption cross section, σ_{abs}, for transition from the ground state $|0\rangle$ with energy E_0 to an excited state $|n\rangle$ with energy E_n, defined as energy absorbed per unit time by the atom, divided by energy flux of the radiation field, is given by (Sakurai, 1994)

$$\sigma_{abs} = \frac{4\pi^2\hbar}{m^2\omega}\left(\frac{e^2}{\hbar c}\right)\left|\left\langle n\left|e^{i\mathbf{k}\cdot\mathbf{r}}\varepsilon\cdot\mathbf{p}\right|0\right\rangle\right|^2 \delta(E_n - E_0 - \hbar\omega), \tag{5.1}$$

where

k = (ω/*c*)***n*** is the wave number vector of the monochromatic light propagating toward ***n*** with polarization vector ε

p the electron momentum operator

r the coordinate of the electron involved in the transition

By the use of dipole approximation combined with the commutation relation $[x, H_0] = i\hbar p_x/m$, Equation 5.1 is transformed to

$$\sigma_{abs} = 4\pi^2\alpha\omega_{n0}\left|\left\langle n\,|\,x\,|\,0\right\rangle\right|^2 \delta(\omega - \omega_{n0}). \tag{5.2}$$

Here, the radiation field is assumed to propagate in the z direction with the polarization vector along the x-axis, $\alpha = e^2/\hbar c$ is the dimensionless fine-structure constant, and $\hbar\omega_{n0} = E_n - E_0$. Atoms and molecules have many excited states, and hence their response to white light is represented by simply integrating the above over all the excited states:

$$\int \sigma_{abs} d\omega = \sum_n 4\pi^2\alpha\omega_{n0}\left|\left\langle n\,|\,x\,|\,0\right\rangle\right|^2. \tag{5.3}$$

In atomic and molecular physics it is common to use a dimensionless quantity called optical oscillator strength, or simply oscillator strength, defined by

$$f_{n0} \equiv \frac{2m\omega_{n0}}{\hbar}\left|\langle n \mid x \mid 0\rangle\right|^2. \tag{5.4}$$

In terms of the oscillator strength, the Thomas–Reiche–Kuhn sum rule can be expressed in the following simple manner:

$$\sum_n f_{n0} = 1. \tag{5.5}$$

Since Equation 5.5 applies for each electron, the right-hand side becomes N if the system has N electrons. Hence, if oscillator strength distribution (the relative values of f_{n0} for wide energy range) is measured, it can be brought into absolute scale by the use of the sum rule. The energy range is, in principle, from zero to infinity. In practice, measurements can be made only for a limited energy range, and hence we have to know how wide it should be in order to justify the use of the sum rule, as seen in Equation 5.5.

Figure 5.2 shows an IXS or x-ray Raman scattering spectrum of liquid water that, as is described later, is theoretically expected to be similar to the optical absorption spectrum. The signal due to valence electron excitation starts at around energy loss (E) of 7 eV, has a maximum at around 22 eV, and monotonically decays to higher energy. At around 540 eV, a scattering corresponding to oxygen K absorption starts, but the peak intensity is about two orders of magnitude less than that of valence electron excitation. Global profiles of VUV absorption spectra of organic compounds are somewhat similar, except that K absorption of carbon starts at 284 eV; most of the oscillator strength by valence electron excitations distributes between 0 and about 200 eV (Williams et al., 1991).

Photoabsorption spectra on liquids, gases, and solids are routinely measured in the infrared, visible, and UV regions. However, photoabsorption experiments in the VUV (above about 7 eV)

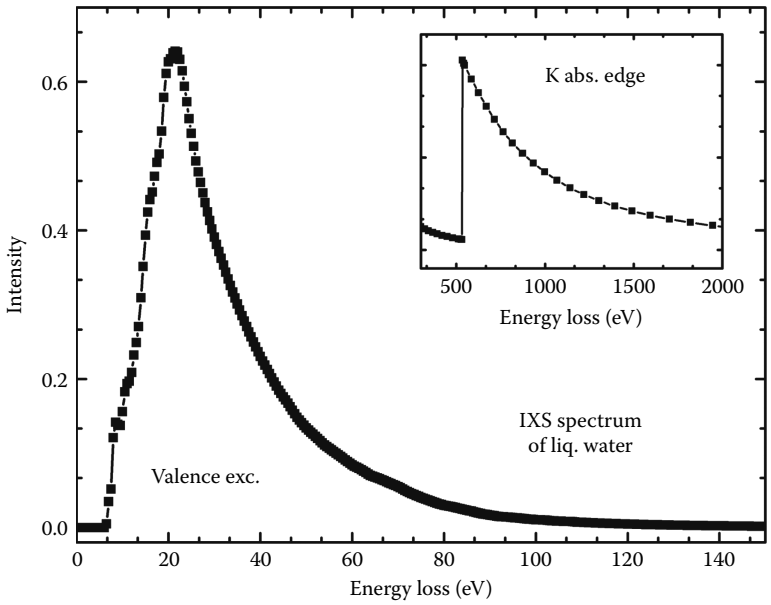

FIGURE 5.2 A hard x-ray inelastic-scattering spectrum of liquid water at small momentum transfer, which is essentially identical with VUV absorption spectrum (Hayashi et al., 2000). See text following Equation 5.7. The inset, which corresponds to K absorption of oxygen, is based on the NIST photoelectric cross section database for the water molecule (http://physics.nist.gov/ffast).

impose serious difficulties because air strongly absorbs VUV photons and hence measurements have to be carried out in a vacuum. In addition, absorbance of most substances is so high in the VUV that almost no window material is available above around 10 eV. Consequently, the direct absorption method is applicable only for low-pressure gases or very thin films, combined with differential pumping technique. Therefore, instead of direct absorption, reflectance measurements are conventionally employed for VUV studies on condensed phase substances (Seki et al., 1981; Kobayashi, 1983; Ikehata et al., 2008). Even with the reflectance method, however, measurements of the optical spectra of volatile liquids present a further difficulty, namely, how to keep them in vacuum. In an effort to obtain optical functions in the VUV, Heller et al. measured the reflectance spectrum from free-water surface kept in an open dish cooled to 1°C in near-vacuum conditions made with two stages of differential pumping; each stage included a cryopump capable of pumping 80,000 L of water vapor per second (Heller et al., 1974). Still, the spectral range measured was limited to below 25.6 eV. Hence, in order to evaluate optical functions, they had to resort to extrapolation, assuming either exponential or power functions. They estimated errors in optical constants due to the extrapolation to be as large as 20% above 20 eV. To the best of our knowledge, no VUV absorption study on liquid water for wide energy range has been reported since the 1970s, in spite of recent advancements in VUV technology.

In this respect, however, it may be worth mentioning here that very recently an absorption spectrum of liquid water in a very narrow range (530–545 eV, corresponding to the onset of K absorption in Figure 5.2) was observed by monitoring Kα fluorescence from oxygen at 525 eV (Myneni et al., 2002). Liquid water was kept in a He atmosphere at a pressure of 760 Torr and was separated from the high vacuum of a beam line by a Si_3N_4 window. This method can be employed neither for valence electron excitation nor for observation of wide energy range in question here, but it suggests that some day improvements of light sources, detectors, or window materials may make direct observation of VUV absorption possible.

5.3 INELASTIC X-RAY SCATTERING AND GENERALIZED OSCILLATOR STRENGTH

Inelastic x-ray as well as electron scatterings can provide a wealth of information, a part of which is equivalent to the optical oscillator strength distribution. The basic principle of a typical IXS process is sketched in Figure 5.3. A photon of energy $\hbar\omega_0$, momentum $\hbar\mathbf{k}_0$, and polarization vector ε_0 impinges upon a target and is inelastically scattered by an angle θ into a photon of energy $\hbar\omega_1$, momentum $\hbar\mathbf{k}_1$, and polarization vector ε_0. Concomitantly, the target undergoes a transition from the initial state $|0\rangle$ with energy E_0 to an excited state $|n\rangle$ with energy E_n. The energy $E = \hbar(\omega_0 - \omega_1)$ and the momentum $\hbar\mathbf{q} = \hbar(\mathbf{k}_0 - \mathbf{k}_1)$ are transferred to the target.

The double differential scattering cross section for IXS of isotropic materials such as gases and liquids is expressed as follows (Bonham, 2000):

$$\frac{d^2\sigma}{d\Omega dE} = r_0^2 \left(\frac{\omega_1}{\omega_0}\right)(\varepsilon_0 \cdot \varepsilon_1)^2 \left(\frac{q^2}{E}\right)\frac{df(q,E)}{dE}, \tag{5.6}$$

where

$$\frac{df(q,E)}{dE} = \frac{E}{q^2}\sum_n \left\langle \left| \left\langle n \left| \sum_j^N \exp(i\mathbf{q}\cdot\mathbf{r}_j) \right| 0 \right\rangle \right|^2 \right\rangle_\Omega \delta(E-(E_n - E_0)) \tag{5.7}$$

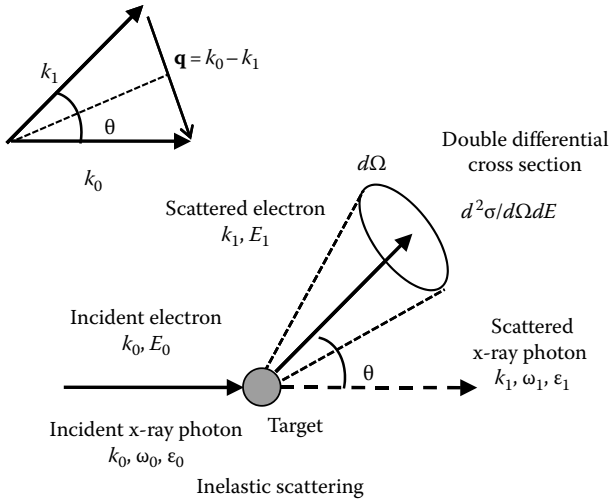

FIGURE 5.3 A schematic diagram of inelastic-scattering processes of x-ray photons and electrons.

defines the generalized oscillator strength (GOS), which is an extension of the optical oscillator strength and is often used in atomic and molecular physics. Here r_0 is the classical electron radius ($=e^2/mc^2$), $\langle - - - \rangle_\Omega$ means orientation average, and $d\Omega$ corresponds to the solid angle. The summation about n is over all the excited states, discrete as well as continuum. N is the number of electrons in the target system and $\mathbf{r}_j$ is the instantaneous position of the jth electron.

Equation 5.6 is quite general. Depending on the magnitude of $qr_j = |\mathbf{q} \cdot \mathbf{r}_j|$, however, IXS spectra show entirely different features. In the case $qr_j \gg 1$, that is, the momentum transfer $q = |\mathbf{q}|$ is large, and/or the electron involved in the process is loosely bound and consequently $r_j = |\mathbf{r}_j|$ is large, the corresponding IXS is the well-known Compton scattering; binding energies of the electrons can be neglected and the spectra are approximated by symmetric parabolas. On the contrary, if the electron is tightly bound and/or q is small and accordingly $qr_j \ll 1$, the binding energy cannot be neglected but energy transfer can. Expanding the exponential into the power series and making use of the orthogonality of the states 0 and n, one can easily see the first non-zero term in the bracket of Equation 5.7 reduces to the same form as that of Equation 5.4. Hence at the limit $qr_j \to 0$, the scattering spectrum becomes identical with the corresponding x-ray absorption spectrum. IXS under these conditions are sometimes called x-ray Raman scattering and can be a substitute of soft x-ray and VUV absorption (Tohji and Udagawa, 1989; Bowron et al., 2000). In between, that is, $qr_j \sim 1$, both the binding energy and momentum transfer should be taken into consideration, providing GOS that depends both on momentum transfer as well as energy.

The GOS at any momentum transfer can be made absolute by using the following Bethe sum rule (Bethe and Jackiw, 1968; Inokuti, 1971):

$$\int \frac{df(q,E)}{dE} dE = N, \tag{5.8}$$

where N is the total number of electrons in the target.

In solid state physics, it is more common to use a quantity slightly different from GOS called the dynamic structure factor $S(\mathbf{q}, E)$, defined by the following equation:

$$S(\mathbf{q},E) = \frac{q^2}{E}\frac{df(\mathbf{q},E)}{dE} = \sum_n \left| \left\langle n \left| \sum_j \exp(i\mathbf{q}\cdot\mathbf{r}_j) \right| 0 \right\rangle \right|^2 \delta(E - (E_n - E_0)). \tag{5.9}$$

In isotropic substances, the dielectric function depends only on the magnitude of the momentum transfer q. Dynamic structure factor can be written in terms of the macroscopic dielectric response function $\varepsilon(q,E)$ through the fluctuation-dissipation theorem (Pines, 1964) by

$$S(q,E) = \frac{\hbar q^2}{4\pi^2 e^2 n_e} \operatorname{Im}\left[\frac{-1}{\varepsilon(q,E)}\right]_{\hbar\omega=E}, \tag{5.10}$$

where n_e is the average electron density in the material. The function at the right-hand side of Equation 5.10, namely,

$$\operatorname{Im}\left[\frac{-1}{\varepsilon(q,E)}\right] = \frac{\varepsilon_2(q,E)}{\varepsilon_1^2(q,E)+\varepsilon_2^2(q,E)}, \tag{5.11}$$

plays a central role in the theory of the interaction between charged particles and the media, and is often called energy loss function (ELF). While the numerator in Equation 5.11 corresponds to single-particle transitions of an isolated atom or molecule, the denominator accounts for the influence of the condensed phase, that is, shielding or screening effect. The real part of the dielectric function can be derived from ELF by making use of the well-known Kramers–Kronig transformation as follows:

$$Re\left[\frac{1}{\varepsilon(q,E)}\right] = 1 + \frac{2}{\pi} P \int_0^\infty \frac{\operatorname{Im}\left[\varepsilon^{-1}(q,E')\right]}{E'^2 - E^2} E' dE'. \tag{5.12}$$

In short, IXS can provide q- and E-dependent GOS or ELF, ultimately leading to real and imaginary parts of complex dielectric function. In a special case, $qr \to 0$, the spectrum is essentially identical to the optical spectrum.

5.4 INELASTIC ELECTRON SCATTERING AND GENERALIZED OSCILLATOR STRENGTH

As was described already, photoabsorption of a matter is closely related to interactions between moving charged particles and the matter. Figure 5.1 is, however, an oversimplified picture and in fact energy as well as momentum is transferred to the target. Such a phenomenon is called collision, a schematic diagram of which is also included in Figure 5.3. Theoretically it is well described by the first Born approximation, and the double differential scattering cross section for isotropic substances is given by the following equation (Bethe and Jackiw, 1968; Bonham and Fink, 1974):

$$\frac{d^2\sigma}{d\Omega dE} = \frac{k_1}{k_0 q^2} \frac{4}{E} \frac{df(q,E)}{dE}, \tag{5.13}$$

where the notation is the same as Equation 5.6. That is, GOS can also be obtained from EELS studies. It should be noted that Equation 5.13 is inversely proportional to q^2, and hence the cross section becomes smaller with increasing momentum transfer. EELS spectroscopy is now an established technique (Bonham and Fink, 1974; Egerton, 1996) and has been widely employed for studies on gaseous atoms, molecules, and solid surfaces, and provides data to complement those obtained by IXS as is demonstrated later.

5.5 GOS MEASUREMENTS BY IXS

As already stated, IXS spectroscopy has unique experimental advantages: a vacuum is not required, various kinds of window materials are available, it is free from charge-up phenomenon, contamination of higher order reflection is insignificant, and bulk properties can be obtained. In the past, however, very low scattering intensities hindered one from obtaining accurate IXS spectra.

Recent advancements of synchrotron radiation (SR) facilities have made it possible to carry out a number of experiments that were impossible with conventional x-ray sources, and IXS measurement is one of them. At beam lines of SR facilities, intense, brilliant, polarized, and monochromatic hard x-rays are available. Still, inelastically scattered x-rays are so weak that they must be collected and monochromatized as efficiently as possible. Since the GOS is a normalized quantity, no absolute measurements of the scattering intensities, or solid angle, or sample concentration are required to obtain absolute values. Instead, what is required is the accuracy of relative intensities within a scattering spectrum and is the observation over a wide-enough energy range.

To obtain quality IXS spectra, two approaches have been employed: the use of a spherically or cylindrically bent dispersing crystal to collect as large a solid angle as possible, and the use of a multidimensional detector to improve sensitivity. The two can be combined too. Two examples, a schematic of the beamline X21 of National Synchrotron Light Source in the United States and of BL16X at Photon Factory at KEK in Japan are shown in Figure 5.4.

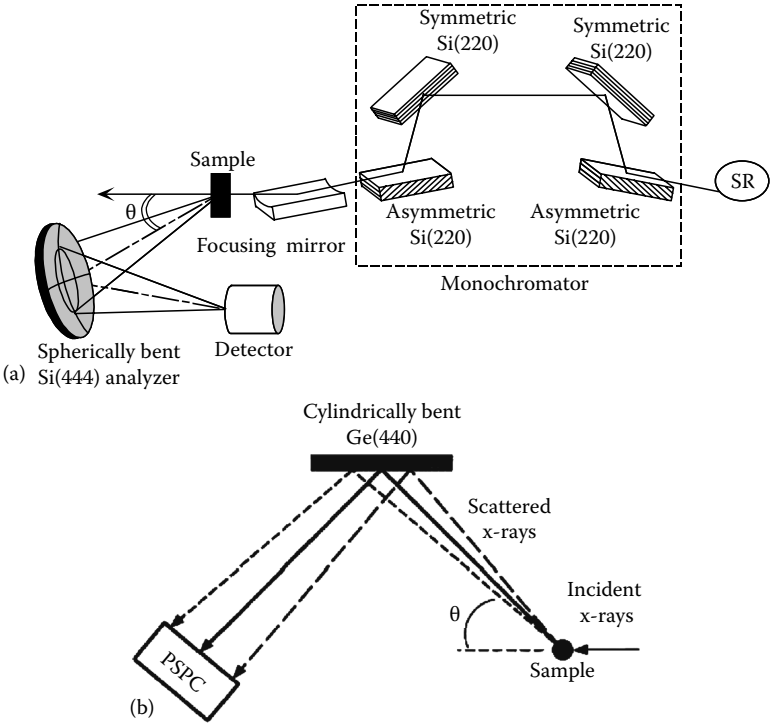

FIGURE 5.4 (a) Schematic diagram of the IXS system at National Synchrotron Light Source beam line X21 of NSLS, Brookhaven National Laboratory, United States (Hayashi et al., 2000). White x-rays from storage ring are monochromatized with a monochromator consisting of four Si(220) crystals and are focused on the sample. A spherically bent Si(444) analyzer is employed as an analyzer. The pass energy of the analyzer is fixed and incident x-ray energy is scanned. (b) Schematic diagram of the analyzer employed at BL16A of Photon Factory, KEK, Japan (Watanabe et al., 1997). Incident x-ray energy is fixed and scattered x-rays are vertically focused and horizontally dispersed with respect to the scattering plane with a cylindrically bent Ge(440) crystal. They are detected with a position-sensitive proportional counter (PSPC) combined with a multichannel analyzer, thus eliminating any effects due to variation in intensity of the incident x-rays.

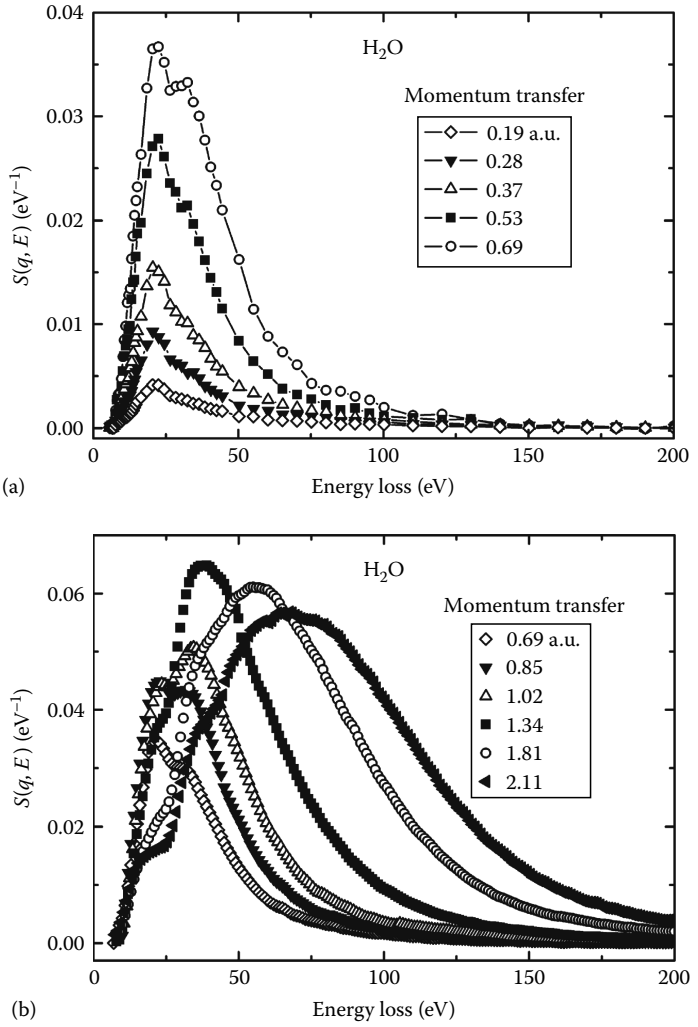

FIGURE 5.5 Normalized $S(q, E)$ spectra from $q = 0.19$ to 0.69 a.u. (a) and those from $q = 0.69$ to 2.79 a.u. (b).

Figure 5.5a and b shows normalized $S(q,E)$ spectra from q = 0.19 to 0.69 atomic unit (1 a.u. = $\hbar/a_0$, a_0: Bohr radius = 0.529×10^{-11} m) collected at X21 of NSLS and those from q = 0.69 to 2.79 a.u. at BL16A of Photon Factory. For those shown in Figure 5.5a, normalization was made by using the theoretically calculated static structure factor $S(q) = \int S(q,E)dE$ (Wang et al., 1994; Hayashi et al., 1998). In order to normalize the spectra shown in Figure 5.5b where the tails extend to higher energy loss, the data were least-squares fitted to the function A/E^b over the energy region 100–250 eV for q less than 2.9 a.u. and 300–420 eV for q larger than 2.9 a.u. (not shown in the figure), and extrapolated to infinity. The total area was then normalized to a value of 8.34, which corresponds to the total number of valence electrons (8) plus a small correction (0.34) for the Pauli-excluded transitions from the oxygen K shell electrons to the already occupied valence shell orbitals (Chan et al., 1993). The spectral shapes of $S(q,E)$ at q = 0.69 a.u. in Figure 5.5a and b agree quite well with each other, indicating that the measurements as well as normalizations were properly made at both SR facilities.

In atomic and molecular physics, it is more common to use GOS or ELF than dynamic structure factor. The three-dimensional representation of ELF or GOS vs. E and q, like the one shown in

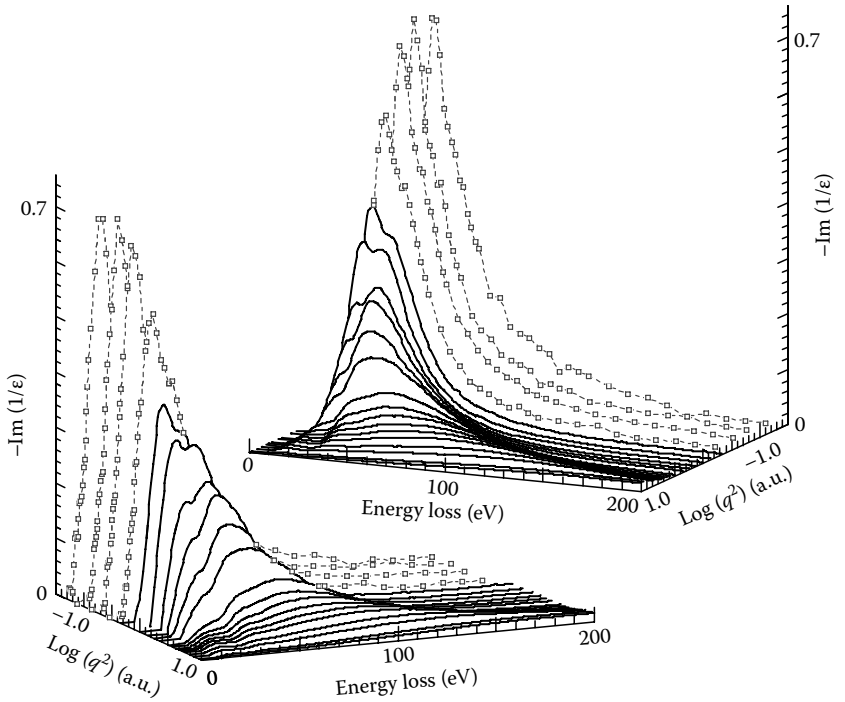

FIGURE 5.6 Experimental Bethe surface of liquid water viewed from two different directions. Squares, data obtained at X21 of NSLS; solid lines, data obtained at BL16A of PF.

Figure 5.6, gives a surface, named Bethe surface by Inokuti, which contains all the information about the inelastic scattering of fast charged particles by the atom or molecule within the first Born approximation (Inokuti, 1971). For small values of momentum transfer, the form of the surface resembles a photoabsorption spectrum, having a peak at around 22 eV. With increasing momentum transfer, the Bethe ridge, that is, the range of the peaks at around $E = \hbar q^2/2m$, shifts to the high energy and the shape gets broader and closer to symmetric, that is, it becomes Compton scattering like.

5.6 OPTICAL LIMIT

Now we have experimentally obtained energy and momentum dependence of dynamic structure factor $S(q,E)$, GOS, or ELF of liquid water in absolute scale for a wide range of energy and momentum transfers. They can easily be converted to dielectric function through Equations 5.10 and 5.12. Unfortunately, however, no other experimental data exist that can be utilized to make comparisons in order to examine the accuracy of the results presented in Figure 5.6. However, comparisons can be made in a special case for $q = 0$, because Equation 5.7 predicts that GOS, ELF, and dielectric function all converge as q approaches zero and become identical with those deduced from optical measurements. In the following, whether or not the optical limit is achieved under the experimental conditions employed is first examined, and subsequently optical constants and functions derived from IXS data under the optical limit are compared with corresponding ones at visible and near-UV regions.

The ELFs of liquid water are plotted for several q's in Figure 5.7, which clearly demonstrates that they converge with decrease in q, approaching the optical limit. Those for $q = 0.28$ a.u. and for $q = 0.19$ a.u. overlap within the experimental error; thus, they both can be regarded as the ELF at $q = 0$, that is, Im $[-1/\varepsilon(0,E)]$. Figure 5.8 shows the ELF at $q = 0.28$ a.u. for a much wider range together with the one derived from a reflectance measurement (Heller et al., 1974). The shape of the two resemble each other, but the maximum values differ considerably, 0.65 vs. 1.1. The difference has a significant effect on the absolute values of dielectric response functions.

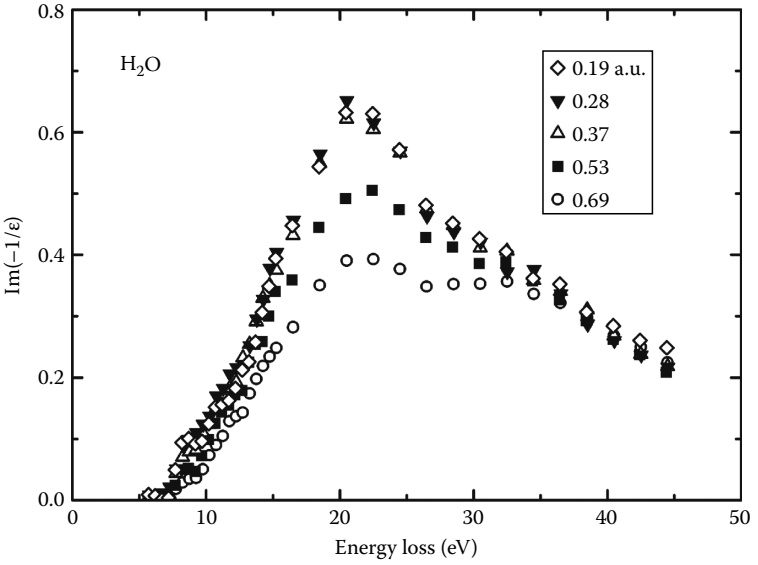

FIGURE 5.7 The ELF, Im[−1/ε(q, E)], of liquid water plotted for 0.19 a.u. ≤q≤0.69 a.u.

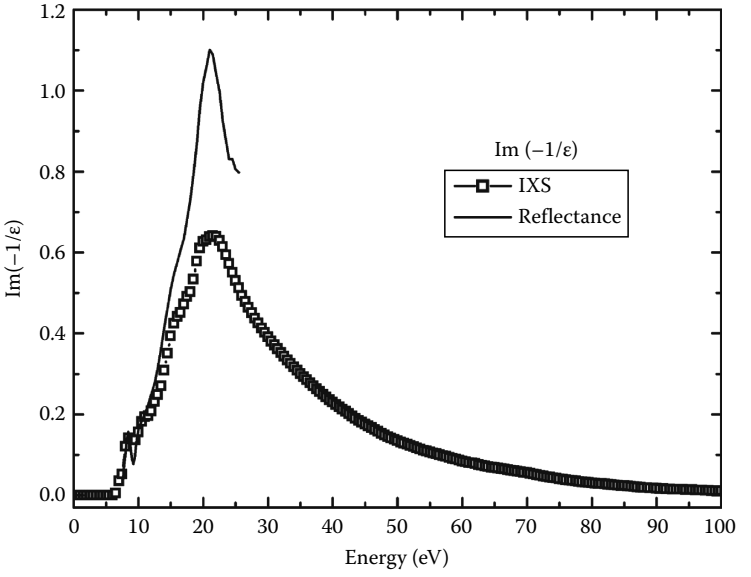

FIGURE 5.8 The ELF, Im[−1/ε(0, E)], derived from IXS. That from the reflectance measurement (Heller et al., 1974) is also shown.

Real (ε_1) as well as imaginary (ε_2) parts of the dielectric response function $\varepsilon(0,E)$ of liquid water derived by the use of Kramers–Kronig relation are shown in Figure 5.9. Several values of ε_1 calculated from the well-documented refractive index of water in the visible and near-UV region are indicated in the figure by the solid squares. All the squares fall almost exactly on the observed curve, which endorses the accuracy of the present results.

Also shown in Figure 5.9 are the real and imaginary parts of the dielectric response functions derived from reflectance (Heller et al., 1974). As far as the global shapes are concerned, they show a qualitative agreement with those of ours, but again quantitatively there are substantial differences. The most significant difference lies in the behavior of ε_1 where ELF shows a maximum.

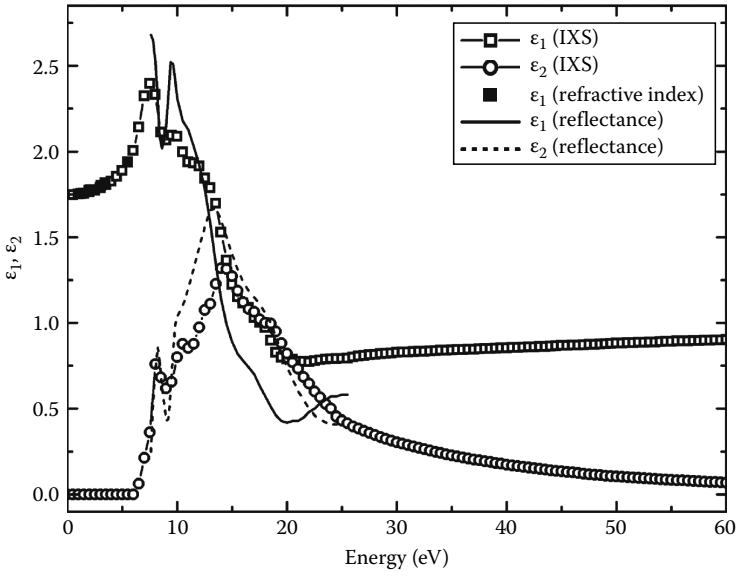

FIGURE 5.9 Real (ε_1) and imaginary (ε_2) parts of the dielectric function of liquid water determined with IXS (Watanabe et al., 1997) and those from reflection (Heller et al., 1974). Closed squares are ε_1 calculated from index of refraction.

While in Heller's results ε_1 displays a distinct valley with a minimum value of 0.42, ours has barely observable minimum with a value of 0.75. It has been a matter of debate whether or not the peak of ELF at 21–22 eV is plasmon-like collective excitation (Heller et al., 1974; Kaplan, 1995). The observation here supports the hypothesis that the peak, though of some collective character, is not due to a plasmon excitation (La Verne and Mozumder, 1993), because ε_1 does not make a deep valley and cannot be regarded to be much smaller than 1 at the peak energy of ELF. As the energy increases, ε_1 gradually approaches 1 from below and ε_2 monotonically decreases toward zero until K absorption starts.

The optical oscillator strength distribution of liquid water from IXS is shown in Figure 5.10 together with estimated uncertainties. The ordinate scale is absolute. Except for a small shoulder at around 8 eV and another less distinct one at around 11 eV, the oscillator strength distribution of liquid water increases sharply with increasing energy, reaches a peak at around 22 eV, and then decreases monotonically.

Figure 5.10 also shows the optical oscillator strength distribution of gaseous water obtained by EELS (Chan et al., 1993). The gas phase spectrum is characterized by sharp absorption bands followed by continuum above ionization threshold (12.6 eV), but the data shown here were obtained at 1 eV resolution and hence the structures are a convolution of many sharp lines. In the liquid state, sharp absorption features are lost and the entire oscillator strength distribution shifts toward the higher energy side. This reflects the fact that in condensed phases, excited electrons are somewhat limited in space (Inokuti, 1991). As the energy increases, the oscillator strength distributions of gaseous water and liquid water get closer as expected. This is because the shielding factor $\varepsilon_1^2 + \varepsilon_2^2$ reaches almost 1 at high energies, reflecting the fact that ε_1 and ε_2 monotonically approach 1 and 0 at higher energies until K absorption starts at 540 eV.

The absolute oscillator strength distributions of two forms of ice can be calculated from the reflection spectra on hexagonal ice at 80 K (Seki et al., 1981; Kobayashi, 1983) and that from the EELS spectrum on amorphous ice at 78 K (Daniels, 1971), both up to about 28 eV. They are shown in the inset of Figure 5.8 together with those of liquid as well as gaseous water. For hexagonal ice, a distinct peak is observed at 8.7 eV, followed by several other structures at higher energy. In contrast, these structures are broadened and less well-defined in amorphous ice. In fact, the oscillator strength distribution of amorphous ice almost overlaps with that of liquid water; both the peak

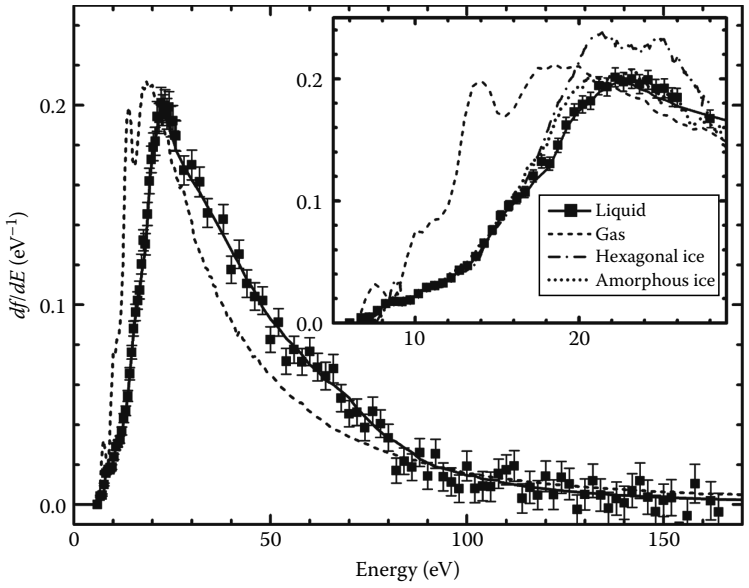

FIGURE 5.10 Oscillator strength distribution of liquid water, gas phase water (Chan et al., 1993), hexagonal ice, and amorphous ice.

energy of the oscillator strength distribution and its magnitude are almost identical for the two systems. This similarity has been confirmed elsewhere (Emfietzoglou et al., 2006a). Amorphous ice bears a similar molecular layout to that of liquid water, and thus the optical spectra of these two media are expected to be rather similar. In other words, taking into consideration that one is from EELS on ice and the other is on liquid water from IXS, the agreement cannot be fortuitous and it presents one of the evidences to prove an accuracy of the present IXS measurements.

5.7 COMPARISON OF GOS FROM EELS AND IXS

GOS can be obtained from EELS experiments on gaseous molecules. GOS studies on gas phase water have been first reported by Lassettre et al. and later by Takahashi et al. (Lassettre and Skerbele, 1974; Lassettre and White, 1974; Takahashi et al., 2000). In the former study, the incident kinetic energy was about 500 eV, and hence the momentum transfer and energy loss ranges were limited to below 1.5 a.u. and 75 eV, respectively. The elastic scattering intensities were employed for normalization. In the latter, the incident electron energy was 3 keV, and hence measurements were carried out for much wider momentum and energy transfer range, that is, up to 3.5 a.u. and 400 eV. The data were normalized by the use of the sum rule. Figure 5.11a and b compares GOS of the two studies at energy losses of 25 and 45 eV. In spite of the difference in incident energy and normalization method, the results agree quite well wherever the comparison can be made.

Figure 5.11a–e also compares GOSs of the gas phase water by EELS and liquid water by IXS for a wider momentum and energy transfer range. It is clear from the figure that they almost coincide in absolute scale at every energy loss examined. Considering that EELS and IXS are completely different experimental techniques and made on water in different phases, the agreement is rather striking and endorses that both measurements were properly carried out. Furthermore, it can be concluded that single-particle excitation prevails over collective excitation in the momentum transfer range studied here (0.69 a.u. $< q <$ 3.59 a.u.). It is rational, because 0.69 a.u. in momentum space corresponds to about 0.08 nm in position space, which is much smaller than the van der Waals radius of water molecule. The results here suggest that "gas phase approximation," where a simple extrapolation of gas phase data to unit density is employed (Paretzke, 1987), is fairly good except for very small q.

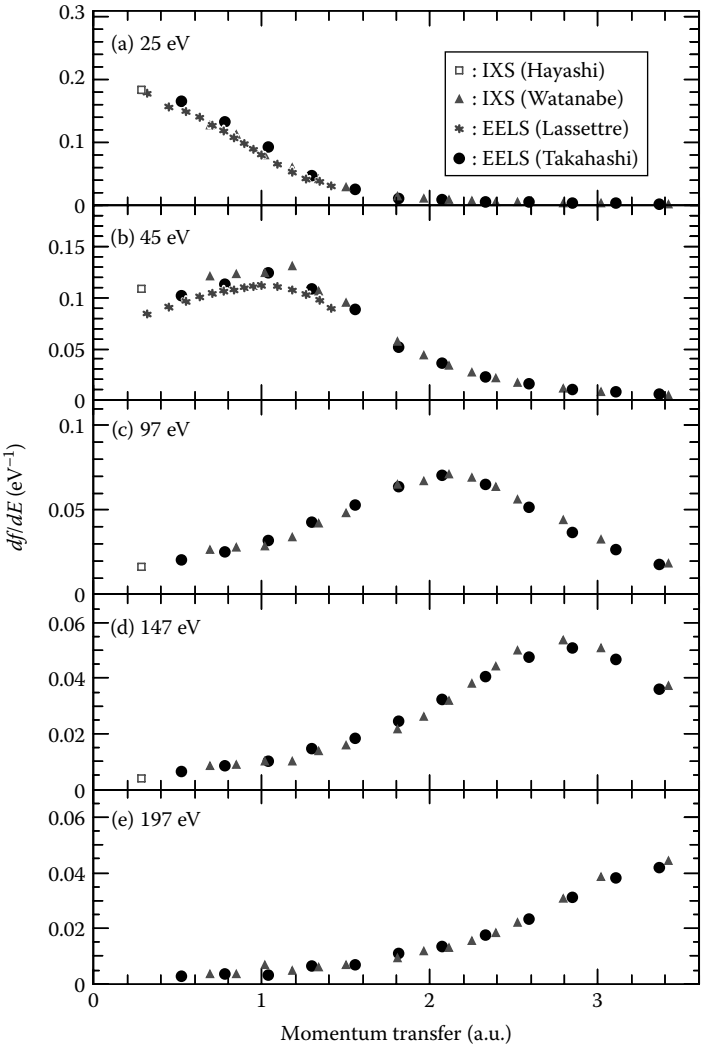

FIGURE 5.11 Comparison of the GOSs by EELS and IXS at several energy loss values.

5.8 BETHE SURFACE OF LIQUID WATER

Dielectric response function $\varepsilon(\omega, q)$ is, as has been stressed already, the central quantity governing various properties of a material and is best presented as a Bethe surface. Bethe surfaces of molecules can in principle be obtained by ab initio calculations, but in practice, the calculation from the first-principles is a formidable task for realistic materials. Hence, apart from the atomic hydrogen and the free electron gas, theoretical construction of Bethe surface of liquid water has so far been made semi-empirically (Dingfelder and Inokuti, 1999; Emfietzoglou et al., 2005, 2006b, 2008a,b). Most studies start with an analytic representation of the experimental optical data $\mathrm{Im}[-1/\varepsilon(0,E)]$, which fulfill the sum rule. Subsequently, momentum dependence is introduced by assuming various dispersion models. Though physically plausible models are contrived and elaborated, calculations based on the processes described above had generally been viewed as tentative because there had been no way to test the accuracy of the q-dependence until the data presented in Figure 5.6 were reported.

Now experimental Bethe surface of liquid water is known between 0.19 a.u. $< q <$ 2.79 a.u and $0 < E <$ 150 eV. Figure 5.12a shows the experimental Bethe surface with much finer meshes

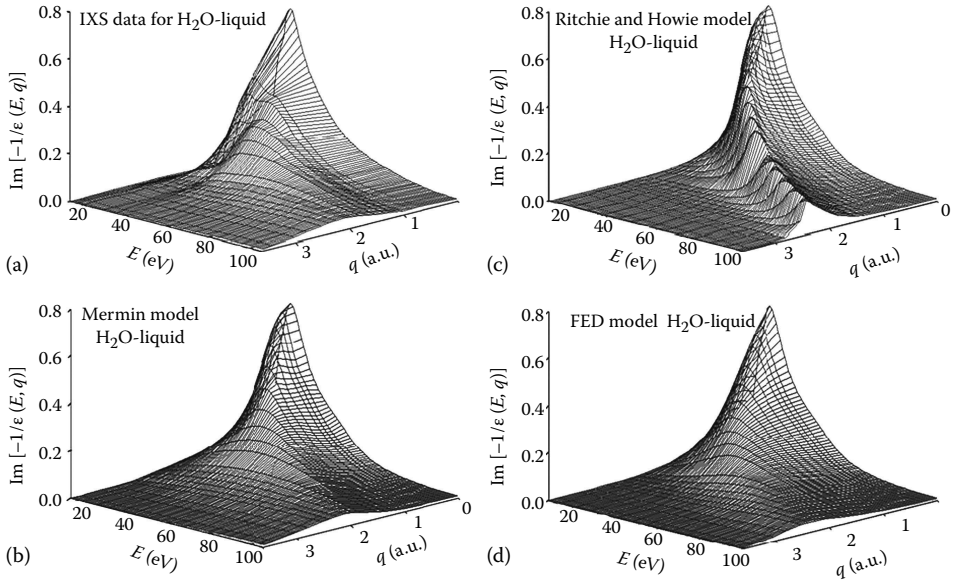

FIGURE 5.12 Observed Bethe surface of liquid water by IXS (a), and calculated ones by Mermin model (b), Ritchie and Howie model (c), and fully extended Drude model (d). (Reprinted from Emfietzoglou, D. et al., *Nucl. Instrum. Methods B*, 266, 1154, 2008b. With permission).

calculated by extrapolation of the IXS data. Figure 5.12b–d presents three examples of calculated Bethe surface of liquid water (Emfietzoglou et al., 2008b). In all the calculations, the ELF shown in Figure 5.8 is fitted by a superposition of five Drude functions (corresponding to excited states) and five derivative Drude functions (ionized states), and subsequently different q-dependence models were assumed. Although all the models reproduced the global characteristics of the experimentally observed Bethe surface, there are obvious differences in the way the Bethe ridge develops.

Figure 5.12c employs the very popular Ritchie and Howie model that assumes a simple quadratic dispersion (Ritchie and Howie, 1977). It is evident that the Bethe ridge is emphasized too much compared with that from IXS observation, Figure 5.12a. That the Bethe ridge is not so steep is supported also from EELS data in Figure 5.11, and hence other models must be looked for. Two model calculations that almost reproduce the experimental Bethe surface are presented and are shown in Figure 5.12b and d. Dependences of some physical quantities on varied optical data and on momentum dispersion models have been studied (Emfietzoglou and Nikijoo, 2005).

5.9 CONCLUDING REMARKS

The dielectric response function $\varepsilon(q, \omega)$ fully describes the interaction of matter and photons or charged particles. For volatile liquids, only IXS experiment can provide $\varepsilon(q, \omega)$ data for finite values of momentum transfer, but because of weak intensity of IXS, not many studies have been reported so far. In condensed phases, intermolecular interactions tend to broaden and smear characteristic low-energy peaks often observed for gas phase molecules. Hence, what is required to extend IXS studies to various other condensed systems is not high resolution but high sensitivity over a wide energy region. In this decade, impressive progress has been made in various aspects of x-ray techniques, and every year, new, more improved monochromators have been commissioned (Bergmann et al., 2002; Hayashi et al., 2004, 2008; Welter et al., 2005; Fister et al., 2006; Huotari et al., 2006; Hudson et al., 2007). It will now be possible to apply IXS to probe dielectric properties of various liquids of interest such as supercritical fluids, ionic fluids, electrolytes, as well as high-pressure gases.

ACKNOWLEDGMENTS

The authors are grateful to Dr. N. Watanabe of IMRAM, Tohoku University and Dr. C.-C. Kao of NSLS for their collaboration.

REFERENCES

Bergmann, U., Glatzel, P., and Cramer, S. P. 2002. Bulk-sensitive XAS characterization of light elements: From x-ray Raman scattering to x-ray Raman spectroscopy. *Microchem. J*. 71: 221–230.

Bethe, H. A. and Jackiw, R. 1968. *Intermediate Quantum Mechanics*, 2nd edn. New York: Benjamin.

Bonham, R. A. 2000. Corrections to the x-ray incoherent scattering factor to obtain the total inelastic x-ray scattering. *J. Mol. Struct. (Theochem)* 527: 103–111.

Bonham, R. A. and Fink, M. 1974. *High Energy Electron Scattering*. New York: van Nostrand Reinhold.

Bowron, D. T., Krisch, M. H., Barnes, A. C., Finney, J. L., Kaprolat, A., and Lorenzen, M. 2000. X-ray-Raman scattering from the oxygen K edge in liquid and solid H_2O. *Phys. Rev. B* 62: R9223–R9227.

Chan, W. F., Cooper, G., and Brion, C. E. 1993. The electronic spectrum of water in the discrete and continuum regions. Absolute optical oscillator strengths for photoabsorption (6–200 eV). *Chem. Phys*. 178: 387–400.

Daniels, J. 1971. Bestimmung der optischen konstanten von eis aus energie-verlustmenssungen von schnellen elektronen. *Opt. Commun*. 3: 240–243.

Dingfelder, M. and Inokuti, M. 1999. The Bethe surface of liquid water. *Radiat. Environ. Biophys*. 38: 93–96.

Dingfelder, M., Hantke, D., Inokuti, M., and Paretzke, H. G. 1998. Electron inelastic-scattering cross sections in liquid water. *Rad. Phys. Chem*. 53: 1–18 and references therein.

Egerton, R. F. 1996. *Electron Energy-Loss Spectroscopy in the Electron Microscope*, 2nd edn. New York: Plenum Press.

Emfietzoglou, D. and Nikijoo, H. 2005. The effect of model approximations on single-collision distributions of low-energy electrons in liquid water. *Radiat. Res*. 163: 98–111.

Emfietzoglou, D., Cucinotta, F. A., and Nikjoo, H. 2005. A complete dielectric response model for liquid water: A solution of the Bethe Ridge problem. *Radiat. Res*. 164: 202–211.

Emfietzoglou, D., Nikjoo, H., Petsalakis, I. D., and Pathak, A. 2006a. A consistent dielectric response model for water ice over the whole energy-momentum plane. *Nucl. Instrum. Methods B* 256: 141–147.

Emfietzoglou, D., Nikjoo, H., and Pathak, A. 2006b. A comparative study of dielectric response function models for liquid water. *Radiat. Prot. Dosim*. 122: 61–65.

Emfietzoglou, D., Pathak, A., and Moscovitch, M. 2008a. Modeling the energy and momentum dependent loss function of the valence shells of liquid water. *Nucl. Instrum. Methods B* 230: 77–84.

Emfietzoglou, D., Abril, I., Garcia-Molina, R., Petsalakis, I. D., Nikjoo, H., Kyriakou, I., and Pathak, A. 2008b. Semi-empirical dielectric descriptions of the Bethe surface of the valence bands of condensed water. *Nucl. Instrum. Methods B* 266: 1154–1161.

Fister, T. T., Seidler, G. T., Wharton, L., Battle, A. R., Ellis, T. B., Cross, J. O., Macrander, A. T., Elam, W. T., Tyson, T. A., and Qian, Q. 2006. Multielement spectrometer for efficient measurement of the momentum transfer dependence of inelastic x-ray scattering. *Rev. Sci. Instrum*. 77: 063901-1–063901-7.

Hayashi, H., Watanabe, N., Udagawa, Y., and Kao, C.-C. 1998. Optical spectra of liquid water in vacuum UV region by means of inelastic x-ray scattering spectroscopy. *J. Chem. Phys*.108: 823–825.

Hayashi, H., Watanabe, N., Udagawa, Y., and Kao, C.-C. 2000. The complete optical spectrum of liquid water measured by inelastic x-ray scattering. *Proc. Natl. Acad. Sci*. 97: 6264–6266.

Hayashi, H., Kawata, M., Takeda, R., Udagawa, Y., Watanabe, Y., Takano, T., Nanao, S., and Kawamura, N. 2004. A multi-crystal spectrometer with a two-dimensional position-sensitive detector and contour maps of resonant Kβ emission in Mn compounds. *J. Electron Spectrosc. Relat. Phenom*. 136: 191–197.

Hayashi, H., Azumi, T., Sato, A., and Udagawa, Y. 2008. A cartography of Kβ resonant inelastic x-ray scattering for lifetime-broadening-suppressed spin-selected XANES of α-Fe_2O_3. *J. Electron Spectrosc. Relat. Phenom*. 168: 34–39.

Heller, Jr., J. M., Hamm, R. N., Birkhoff, R. D., and Painter, L. R. 1974. Collective oscillation in liquid water. *J. Chem. Phys*. 60: 3483–3486.

Hudson, A. C., Stolte, W. C., Lindle, D. W., and Guiemin, R. 2007. Design and performance of a curved-crystal x-ray emission spectrometer. *Rev. Sci. Instrum*. 78: 053101-1–053101-5.

Huotari, S., Albergamo, F., Vanko, G., Verbeni, R., and Monaco, G. 2006. Resonant inelastic hard x-ray scattering with diced analyzer crystals and position-sensitive detectors. *Rev. Sci. Instrum*. 77: 053102-1–053102-6.

Ikehata, A., Higashi, N., and Ozaki, Y. 2008. Direct observation of the absorption bands of the first electronic transition in liquid H_2O and D_2O by attenuated total reflectance far-UV spectroscopy. *J. Chem. Phys*. 129: 234510 and references therein.

Inokuti, M. 1971. Inelastic collisions of fast charged particles with atoms and molecules—The Bethe theory revisited. *Rev. Mod. Phys*. 43: 297–347.

Inokuti, M. 1983. Radiation physics as a basis of radiation chemistry and biology. In *Applied Atomic Collision Physics*, Vol. 4, *Condensed Matter*, S. Datz (ed.), pp. 179–236. New York: Academic Press, Inc.

Inokuti, M. 1986. VUV absorption and its relation to the effects of ionizing corpuscular radiation. *Photochem. Photobiol*. 44: 279–285.

Inokuti, M. 1991. How is radiation energy absorption different between condensed phase and the gas phase. *Radiat. Eff. Defects Solids* 117: 163–167.

Kaplan, I. G. 1995. The track structure in condensed matter. *Nucl. Instrum. Methods B* 105: 8–13.

Kerr, G. D., Cox, Jr., J. T., Painter, L. R., and Birkhoff, R. D. 1971. A reflectometer for studying liquids in the vacuum ultraviolet. *Rev. Sci. Instrum*. 42: 1418–1422.

Kerr, G. D., Hamm, R. N., Williams, M. W., Birkhoff, R. D., and Painter, L. R. 1972. Optical and dielectric properties of water in the vacuum ultraviolet. *Phys. Rev. A* 5: 2523–2527.

Kobayashi, K. 1983. Optical spectra and electronic structure of ice. *J. Phys. Chem*. 87: 4317–4321.

Kutcher, G. L. and Green, A. E. S. 1976. Model for energy deposition in liquid water. *Radiat. Res*. 67: 408–425.

La Verne, J. A. and Mozumder, A. 1993. Concerning plasmon excitation in liquid water. *Radiat. Res*. 133: 282–288.

Lassettre, E. N. and Skerbele, A. 1974. Generalized oscillator strengths for 7.4 eV excitation of H_2O at 300, 400, and 500 eV kinetic energy. Singlet-triplet energy differences. *J. Chem. Phys*. 60: 2464–2469.

Lassettre, E. N. and White, E. R. 1974. Generalized oscillator strengths through the water vapor spectrum to 75eV excitation energy; electron kinetic energy 500 eV. *J. Chem. Phys*. 60: 2460–2463.

Myneni, S., Luo, Y., Naslund, L. A., Cavalleri, M., Ojamae, L., Ogasawara, H., Pelmenschikov, A., Wernet, P., Vaterlein, P., Heske, C., Hussain, Z., Pettersson, L. G. M., and Nilsson, A. 2002. Spectroscopic probing of local hydrogen-bonding structures in liquid water. *J. Phys. Condens. Matter* 14: L213–L319.

Nikjoo, H. and Uehara, S. 2003. Track structure studies of biological systems. In *Charged Particle and Photon Interactions with Matter*, A. Mozunderand and Y. Hatano (eds.), pp. 491–531. New York: Marcel Dekker.

Nikjoo, H., Uehara, S., Emfietzoglou, D., and Cucinotta, F. A. 2006. Track-structure codes in radiation research. *Radiat. Meas*. 41: 1052–1074 and references therein.

Painter, L. R., Birkhoff, R. D., and Arakawa, E. T. 1969. Optical measurements of liquid water in the vacuum ultraviolet. *J. Chem. Phys*. 51: 243–251.

Paretzke, H. G. 1987. Radiation track structure theory. In *Kinetics of Nonhomogeneous Processes*, G. R. Freeman (ed.), pp. 89–170. New York: John Wiley & Sons.

Pines, D. 1964. *Elementary Excitations in Solids*. New York: Benjamin.

Ritchie, R. H. 1982. Energy losses by swift charged particles in the bulk and at the surface of condensed matter. *Nucl. Instrum. Methods* 198: 81–91.

Ritchie, R. H. and Howie, A. 1977. Electron-excitation and optical-potential in electron-microscopy. *Philos. Mag*. 36: 463–481.

Sakurai, J. J. 1994. *Modern Quantum Mechanics, Rev. Edn*. Reading, MA: Addison-Wesley.

Seki, M., Kobayashi, K., and Nakahara, J. 1981. Optical spectra of hexagonal ice. *J. Phys. Soc. Jpn*. 50: 2643–2648.

Smith, J. D., Cappa, C. D., Wilson, K. R., Messer, B. M., Cohen, R. C., and Saykally, R. J. 2004. Energetics of hydrogen bond network rearrangements in liquid water. *Science* 306: 851–853.

Takahashi, M., Watanabe, N., Wada, Y., Tsuchizawa, S., Hirosue, T., Hayashi, H., and Udagawa, Y. 2000. Bethe surfaces and x-ray incoherent scattering factor for H_2O studied by electron energy loss spectroscopy. *J. Electron Spectrosc. Relat. Phenom*. 112: 107–114.

Tohji, K. and Udagawa, Y. 1989. X-ray Raman scattering as a substitute for soft-x-ray extended x-ray-absorption fine structure. *Phys. Rev. B* 39: 7590–7594.

Wang, J., Tripathi, A. N., and Smith, Jr., V. H. 1994. Chemical binding and electron correlation effects in x-ray and high energy electron scattering. *J. Chem. Phys*. 101: 4842–4854.

Watanabe, N., Hayashi, H., and Udagawa, Y. 1997. Bethe surface of liquid water determined by inelastic x-ray scattering spectroscopy and electron correlation effects. *Bull. Chem. Soc. Jpn*. 70: 719–726.

Watanabe, N., Hayashi, H., and Udagawa, Y. 2000. Inelastic x-ray scattering study on molecular liquid. *J. Phys. Chem. Solid* 61: 407–409.

Welter, E., Machek, P., Drager, G., Bruggmann, U., and Froba, M. 2005. A new x-ray spectrometer with large focusing crystal analyzer. *J. Synch. Radiat*. 12: 448–454.

Wernet, P., Nordlund, D., Bergmann, U., Cavalleri, M., Odelius, M., Ogasawara, H., Naslund, L. A., Hirsch, T. K., Ojamae, L., Glatzel, P., Pettersson, L.G.M., and Nilsson, A. 2004. The structure of the first coordination shell in liquid water. *Science* 304: 995–999.

Williams, M. W., Arakawa, E. T., and Inagaki, T. 1991. Optical and dielectric properties of materials relevant to biological research. In *Handbook on Synchrotron Radiation*, Vol. 4, S. Ebashi, S. M. Kochand, and E. Rubenstein (eds.), pp. 95–145. Amsterdam, the Netherlands: Elsevier Science Publisher.